CCFE
CULHAM CENTRE FOR FUSION ENERGY

UK Atomic Energy Authority

UKAEA-CCFE-PR(23)92

Damian Sobieraj, Jan S. Wróbel, Mark R. Gilbert, Andrey Litnovsky, Felix Klein, Krzysztof J. Kurzydłowski, Duc Nguyen-Manh

Composition stability and Cr-rich phase formation in W-Cr-Y and W-Cr-Ti Smart Alloys

Composition stability and Cr-rich phase formation in W-Cr-Y and W-Cr-Ti Smart Alloys

Damian Sobieraj, Jan S. Wróbel, Mark R. Gilbert, Andrey Litnovsky, Felix Klein, Krzysztof J. Kurzydłowski, Duc Nguyen-Manh

This is a preprint of a paper submitted for publication in Metals

MDPI

Article

Composition stability and Cr-rich phase formation in W-Cr-Y and W-Cr-Ti Smart Alloys

Damian Sobieraj [1,‡], Jan S. Wróbel [1,‡*], Mark R. Gilbert [2,‡], Andrey Litnovsky [3,4,‡], Felix Klein [3,‡], Krzysztof J. Kurzydłowski [5,‡] and Duc Nguyen-Manh [2,‡*]

1 Faculty of Materials Science and Engineering, Warsaw University of Technology, ul. Wołoska 141, 02-507 Warsaw, Poland
2 Culham Science Centre, United Kingdom Atomic Energy Authority, Abingdon, Oxon, OX14 3DB, UK
3 Forschungszentrum Jülich GmbH, Institut für Energie- und Klimaforschung, 52425 Jülich, Germany
4 National Research Nuclear University MEPhI, Kashirskoe Sh. 31, 115409 Moscow, Russian Federation
5 Faculty of Mechanical Engineering, Białystok University of Technology, ul. Wiejska 45C, 15-351 Białystok, Poland
* Correspondence: jan.wrobel@pw.edu.pl; (J. S. W.); duc.nguyen@ukaea.uk; (D. N.-M.)
† These authors contributed equally to this work.

Version February 24, 2021 submitted to Journal Not Specified

Abstract: W-Cr-Y smart alloys are potential material candidates for plasma facing components due to their protective behaviour during the loss-of-coolant accident (LOCA), while maintaining beneficial properties of W during the normal operation of the fusion power plant. During plasma exposure the lighter alloying elements are preferentially sputtered at the surface, but in case of a LOCA the plasma quenches and sputtering stops and diffusion of the alloying elements to the surface becomes intensive. The diffusion of Cr to the surface due to alloying elements (Y, Ti) yields a protective oxide layer stopping the sublimation of WO_3. The phase stability and short-range ordering of ternary alloys in W-Cr-Y(Ti) systems has been investigated, using combination of Density Functional Theory (DFT) and Cluster Expansion (CE) methods with Monte-Carlo (MC) simulations. It has been found out from the DFT calculations, that all pairs in the W-Cr-Y system have positive values of the enthalpy of mixing, while most of the Cr-Ti and Ti-W binary structures have negative enthalpies of mixing. The shift in the short-range order as a function of temperature between Cr and W has been predicted as a result of Y addition in W-Cr-Y alloys compared to $W_{70}Cr_{30}$, by around 400 K towards lower temperatures. A strong tendency towards clustering of Y has been observed even at elevated temperatures (1800 K). The decrease of the order-disorder transition temperature (ODTT) as a result of the Y addition has been observed, while the addition of Ti has not shown any significant changes in the ordering of W-Cr-Ti alloys compared to W-Cr alloy. Our MC simulations showed that for the $W_{70}Cr_{29}Y_1$ alloy the enthalpy of mixing (H_{mix}) value is positive in the whole analysed temperature range. Free energy of mixing above 1000 K has been calculated from the first nearest neighbours approximation for $W_{70}Cr_{29}Y_1$ and $W_{70}Cr_{29}Ti_1$ alloys. The results of the present investigations provide an insight enabling for optimizing chemical composition of materials for future plasma facing components.

Keywords: Smart Alloys, Short-Range Order, Plasma-Facing-Materials, W alloys, Cluster Expansion

1. Introduction

Plasma-Facing-Materials (PFM) for the first wall of future fusion power plants are required to possess extraordinary properties while being able to withstand very high temperatures and radiation damage. High melting point, low erosion yield from plasma particles, low tritium retention, resistance towards neutron irradiation, stability during failure/abnormal event are examples of

required properties for potential candidates for fusion DEMO device [1,2]. Currently, tungsten (W) is the leading PFM contender, but its advantages are coupled with brittle failure regimes due to low fracture toughness, which restrict the temperature range at which it could be operating, while also creating several fabrication difficulties. To challenge those obstacles, numerous strategies such as different alloying elements or nanostructure engineered W are being investigated. Binary W-based alloys have been thoroughly investigated with some of them showing deterioration of the mechanical properties whereas for other transmutation induced precipitations were observed under neutron irradiation [3]. Further development of new W-based alloys for PFM is then required to enable the use of fusion energy in future power plants [4].

While the neutron-induced embrittlement and the intrinsic brittleness of W are vital points of research, the safety of the future fusion power plant in case of an accident is another field that should be taken into consideration. The accident scenario involves a total loss of active cooling, referred to as loss-of-coolant-accident (LOCA), and simultaneous air ingress into the vacuum vessel. Due to the nuclear decay heat of the walls the temperature above 1200 K will be reached within three days and remain at those levels for several weeks. Increased temperature and conditions inside the reactor would cause the formation of the volatile WO_3 and the release of radioactive W to the environment. The expected activity of W at the first wall after 5 full power years is 8.74E14 Bq/kg [5]. The passive mitigation of those consequences during the LOCA is crucial and major task towards increased the safety of future fusion power plants.

Smart alloys are potential candidates for plasma facing materials components due to their protective behaviour during the LOCA, while maintaining beneficial properties of W during the normal operation of the fusion power plant. During plasma exposure the lighter alloying elements are sputtered at the surface and as a result there is an almost pure W layer and a concentration gradient in the alloying elements, which causes diffusion of the alloying elements to the surface. Alloying elements are then sputtered again and equilibrium state is reached with a depletion zone of few tens of nanometres. In case of a LOCA the plasma quenches, sputtering stops and diffusion of the alloying elements to the surface becomes intensive because of the onset of intensive oxidation. The diffusion of Cr to the surface due to alloying elements (Y, Ti) yields a protective oxide layer stopping the sublimation of WO_3 [6–9].

Recently a progress has been made in the development and physics understanding of oxidation resistant W-based smart alloys with the addition of Cr as main alloying element to form a protective oxide layer, and Y in concentrations around 1 at.% to support the protective Cr_2O_3 formation and stability [10–13]. Samples in the form of thin films have been deposited using the magnetron sputtering. Measurements proved the feasibility of concept behind W-based smart alloys, as the oxide layers were primary observed to be growing at the surface which decreases the risk of spallation due to volume expansion. It has been also found out, that internal oxides remain immobile and oxygen that passes without reacting, diffuses into the alloy forming internal oxides. Experimental study suggested that the concentration of Y of more than 1.5 at.% destabilizes the protective oxide layer and causes breakaway oxidation. There has been a layer of Y observed at the grain boundaries which reduced the oxidation rate by decreasing the diffusion of O and Cr. In that study it has also been concluded that Y appeared to be stabilizing the Cr-W phase as an effect of grain boundary pinning by nano-particles as well as by the increased solubility of Cr in W originating from the change in the configurational entropy of the system.

Before describing the model that will be used to study the behaviour of ternary W-based alloys, it is useful to consider the relative nuclear response of W and the 3 alloying elements being considered here. Figure 1 shows the predicted evolution in composition of the four different pure elements as if they were exposed to a 2-year continuous (full-power) irradiation under the conditions expected for the first wall of a typical fusion reactor. Here, the neutron flux and spectrum has been taken from predictions in the equatorial outboard first wall of a recent conceptual design for a European demonstration fusion power plant (DEMO, see [14]). 2 years of continuous full power operation is

representative of the overall exposure expected for first wall components in DEMO (which will have pulsed operational campaigns of roughly 5 years between maintenance periods) [15,16]. The inventory code FISPACT-II [17] was used to predict change in composition due to the transmutation, which is shown in the plots by the growth in concentration (defined in units of atomic parts per million or appm) of elements different from the original element (i.e. not W,Cr,Ti, or Y, which are shown as the nearly constant horizontal lines at 1e6 appm in each graph). FISPACT-II, using the latest TENDL nuclear data libraries [18], can also evolve compositions after irradiation during decay cooling and subsequently derive the total activity of the material at each time based on the half-lives of the decaying radionuclides in the composition. Figure 2 shows the results of this activity evolution, measured in Becquerels per kg of each element, for 1000 years after the end of the 2-year exposure.

Figure 1 demonstrates that W suffers the most severe transmutation, potentially growing several atomic % (1e4 appm equates to 1 atomic %) of transmutant elements during exposure. The alloying elements Ti, Cr, Y show at least an order of magnitude lower transmutation rates. Similarly, the activation results (figure 2) show that W produces the highest long-term activity, potentially only just reaching the UK's limit for low-level waste (LLW) [19] 100 years after the end of reactor exposure and having a significant long-term residual activity caused by long-lived states of ^{186}Re (^{186m}Re has a half-life, $T_{1/2}$ of 2×10^5 years). However, at intermediate timescales, ranging from 50 to just over 100 years of decay, pure Y has slightly higher activity than W, Cr, or Fe, with the drop to low-activity delayed by the combined presence of ^{85}Kr ($T_{1/2} = 10.8$ years) and ^{90}Sr (28.8 years) radioisotopes [20]. In the present case, it takes several decades longer for Y to reach the LLW limit than W, even though it is eventually (beyond 200 years) much less active. Thus high concentrations of this element could produce a delay in disposal (or recycling) of a W-alloy. Ti and Cr decay to activities below the LLW limit at least as quickly as W in this simulation (representing one of the most severe exposure conditions in DEMO), and so their use in a W-alloy is unlikely to cause any long-term waste issues in comparison to pure W.

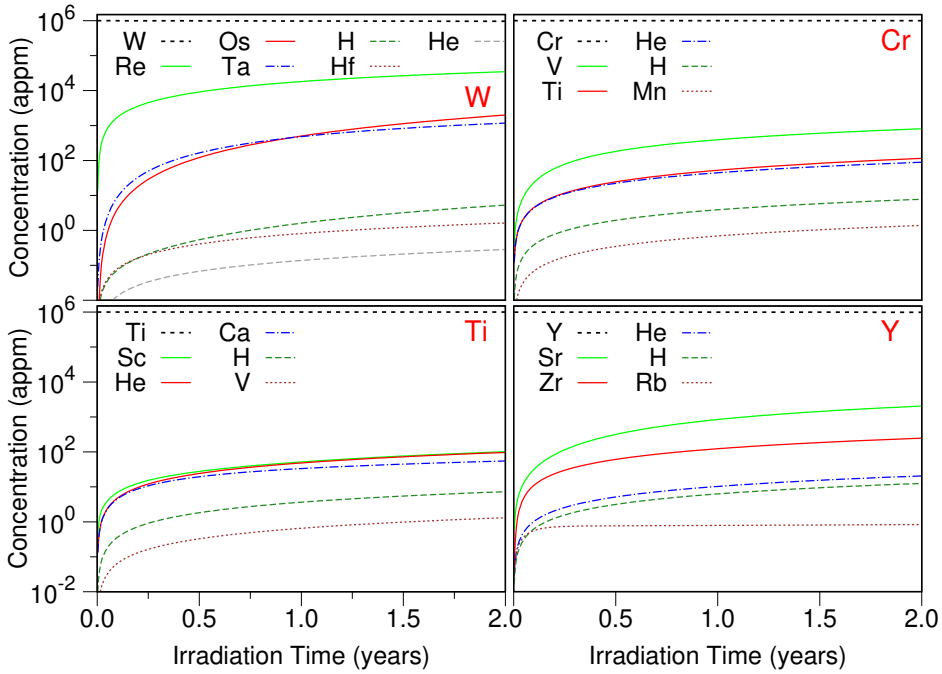

Figure 1. Transmutation (burn-up) response of W, Ti, Cr and Y under a typical fusion first wall irradiation exposure.

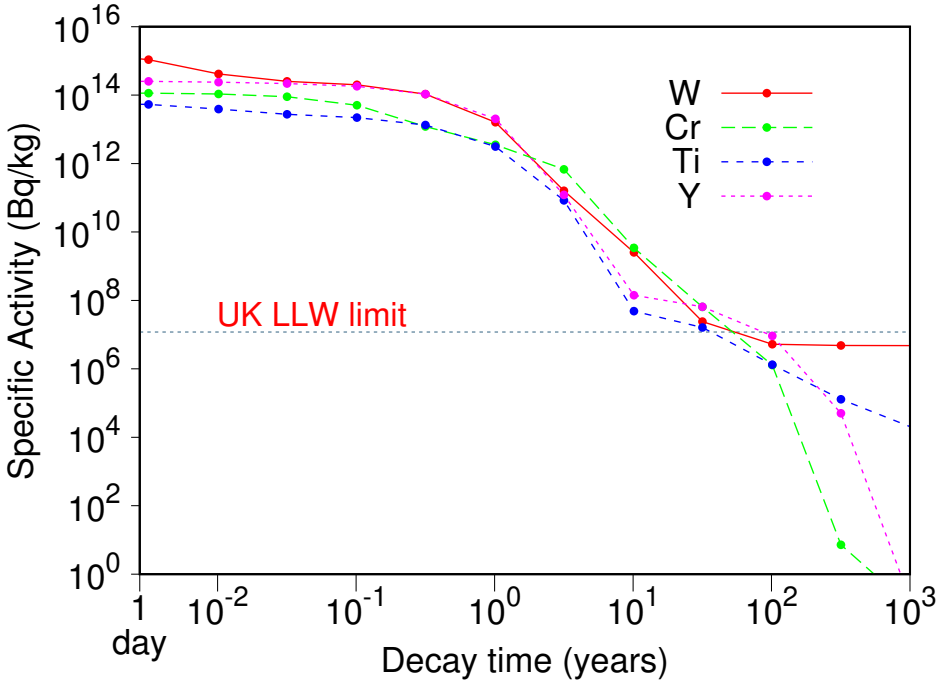

Figure 2. Radiological response represented by total activity in Bq/kg of W, Ti, Cr and Y during decay cooling following a two full power year exposure under typical fusion first wall conditions.

2. Computational methodology

2.1. DFT Computational details

DFT calculations were performed using the projector augmented wave (PAW) method implemented in VASP [21–24]. Exchange and correlation were treated in the generalized gradient approximation GGA-PBE [25]. To accelerate DFT calculations, we used PAW potentials without semi-core p electron contribution. The results of DFT calculations with and without semi-core p electron contributions did not differ [26]. Since the difference between enthalpies of mixing of anti-ferromagnetic and non-magnetic Cr-rich structures was small, the magnetism was not considered in this study. Total energies were calculated using the Monkhorst-Pack mesh [27] of k points in the Brillouin zone, with k-mesh spacing of 0.2 Å^{-1}. This corresponds to 14x14x14 k-point meshes for a two-atom bcc cubic. After initial analysis, the plane-wave cutoff energy used in the calculations was set to 400 eV. The total energy convergence criterion was set to 10^{-6} eV/cell, and force components were relaxed to 10^{-3} eV/Å.

2.2. Cluster Expansion formalism

In our study, we use the enthalpy of mixing to determine the stability of the system. We employ an approach similar to the approach already described for ternary alloys [28]. We define the enthalpy of mixing obtained in DFT calculations of a K-component bcc alloy as a:

$$\Delta H^{bcc}_{mix}(\vec{\sigma}) = E^{bcc}_{tot}(\vec{\sigma}) - \sum_{p=1}^{K} c_p E^{bcc}_{tot}(p) \tag{1}$$

where $E^{bcc}_{tot}(\vec{\sigma})$ is a total energy per atom of the considered alloy in a bcc structure represented by a vector of configurational variables σ, c_p are the average concentrations of each component, and $E^{bcc}_{tot}(p)$ are the total energies of pure elements in a bcc structure. The enthalpy of formation is calculated as the

energy of the structure with respect to the energies of pure element ground states, namely bcc Cr, Y and W.

The enthalpy of mixing of an alloy can also be calculated using the Cluster Expansion method [29–33]:

$$\Delta H^{bcc}_{mixCE}(\vec{\sigma}) = \sum_{\omega} m_\omega J_\omega \langle \Gamma_{\omega'}(\vec{\sigma}) \rangle_\omega, \tag{2}$$

where summation is performed over all clusters ω that are distinct under group symmetry operations applied to a bcc lattice, m_ω are multiplicity factors showing the number of clusters equivalent to ω by symmetry, J_ω are the concentration-independent effective cluster interactions (ECIs), derived from a set of DFT calculations using the structure inversion method, and $\langle \Gamma_\omega, (\overrightarrow{\sigma}) \rangle$ are the average correlation functions defined as a product of point functions of occupation variables on a specific cluster ω averaged over all the clusters ω' that are equivalent by symmetry to cluster ω [34]. Since clusters are defined by their size (a number of lattice points) and the relative positions of points, for clarity, each cluster ω is described by two parameters: $|\omega|$ and n, which refer to the cluster size and the label describing the considered cluster (see Table 1), respectively. In a K-component system, a cluster function is defined as a product of orthogonal point functions $\gamma_{j_i,K}(\sigma_i)$:

$$\Gamma^{(s)}_{\omega,n}(\vec{\omega}) = \gamma_{j_1 K}(\sigma_1)\gamma_{j_2 K}(\sigma_2)\cdots\gamma_{j_{|\omega|} K}(\sigma_{|\omega|}) \tag{3}$$

where $(s) = (j_1, j_2 ... j_{|\omega|})$ is the decoration of the cluster by point functions (see Table 1). The number of possible decorations of clusters by nonzero point functions is a permutation with repetitions equal to $(K-1)^{|\omega|}$. Decorations for $K = 3$ case are being further discussed in the manuscript after Eq. 7. The point functions for a K-component system are defined following [35]:

$$\gamma_{j,K}(\sigma_i) = \begin{cases} 1 & \text{if } j = 0\,, \\ -\cos\left(2\pi\lceil\frac{j}{2}\rceil\frac{\sigma_i}{K}\right) & \text{if } j > 0 \text{ and odd}, \\ -\sin\left(2\pi\lceil\frac{j}{2}\rceil\frac{\sigma_i}{K}\right) & \text{if } j > 0 \text{ and even}, \end{cases} \tag{4}$$

where $\sigma_i = (0, 1, 2, 3, 4, ..., K-1)$ is the index of point functions and $\lceil\frac{j}{2}\rceil$ denotes an operation, where we take the integer plus one value of non-integer value. The 2- and 3-body cluster correlation functions derived from the pair probabilities, are as follows:

$$\langle \Gamma^{(s)}_{2,n} \rangle = \langle \Gamma^{ij}_{2,n} \rangle = \sum_{a=1}^{K}\sum_{b=1}^{K} \gamma_i(\sigma_a)\gamma_j(\sigma_b) y^{ab}_n \tag{5}$$

where y^{ab}_n is the pair probability ($|\omega| = 2$) of finding two atoms a, b in the corresponding shell, denoted by label n.

$$\langle \Gamma^{(s)}_{3,n} \rangle = \langle \Gamma^{ijk}_{3,n} \rangle = \sum_{a=1}^{K}\sum_{b=1}^{K}\sum_{c=1}^{K} \gamma_i(\sigma_a)\gamma_j(\sigma_b)\gamma_k(\sigma_c) y^{abc}_n \tag{6}$$

where y^{abc}_n is the probability of finding 3 atoms a, b and c ($|\omega| = 3$) in the corresponding shell, denoted by label n.

In our study, we have developed the CE Hamiltonian (following explanations for eqs. 2-3) for the ternary bcc Cr-W-Y system (thus $K = 3$), and all the binary bcc subsystems. The enthalpy of mixing for those structures using five smallest 2-body and three smallest 3-body clusters can be written as:

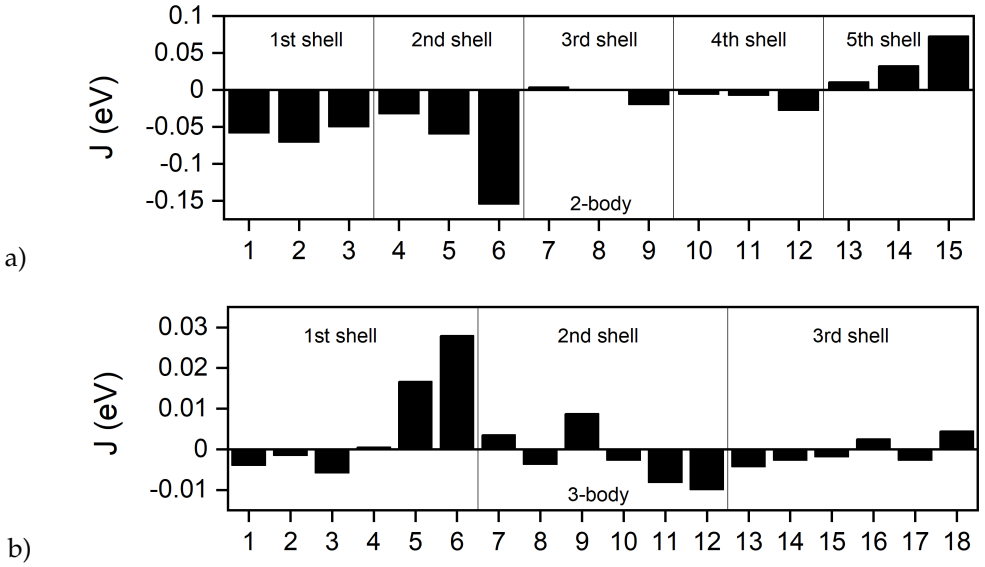

Figure 3. Effective cluster interactions obtained from Cluster Expansion model for a) pairs with up to fifth nearest neighbour and b) three smallest 3-body clusters.

$$\begin{aligned}\Delta H_{mix}(\vec{\sigma}) = & \sum_{\omega,n,s} J^{(s)}_{|\omega|,n} m^{(s)}_{|\omega|,n} \langle \Gamma^{(s)}_{|\omega|,n}(\vec{\sigma}) \rangle = \\ & = J^{(0)}_{1,1} \left\langle \Gamma^{(0)}_{1,1} \right\rangle + \sum_{s} J^{(s)}_{1,1} \left\langle \Gamma^{(s)}_{1,1} \right\rangle + \\ & + \sum_{\mathrm{n}=1}^{5} \sum_{s} m^{(s)}_{2,\mathrm{n}} J^{(s)}_{2,\mathrm{n}} \left\langle \Gamma^{(s)}_{2,\mathrm{n}} \right\rangle + \\ & + \sum_{n=1}^{3} \sum_{s} m^{(s)}_{3,\mathrm{n}} J^{(s)}_{3,\mathrm{n}} \left\langle \Gamma^{(s)}_{3,\mathrm{n}} \right\rangle ,\end{aligned} \tag{7}$$

It should be noted that a summation over all possible decorations of clusters s in Eq. 7 is different for point, pair and 3-body clusters. In a three-component ($K = 3$) system, besides the zero-point function (first term in the second line of Eq. 7), there are 2 non-zero point functions (second term in the second line), which means that there are 2 possible decorations of the point cluster. The cluster of two sites ($|\omega| = 2$) can be decorated in $(K-1)^{|\omega|} = (3-1)^2 = 4$ ways, namely $(s) = (1,1), (1,2), (2,1)$ and $(2,2)$. Due to symmetry reasons $(1,2) = (2,1)$, thus there are 3 required effective cluster interactions to describe the interactions in each 2-body cluster in ternary system (third line in Eq. 7). In a similar way, the number of required effective cluster interactions goes up to 6 for 3-body clusters (fourth line in Eq. 7).

Thirty three ECIs for a 3-component Cr-Y-W system obtained with the CE mapping are given in Figure 3. Fifteen 2-body and eighteen 3-body interaction parameters were derived (pairs with up to fifth nearest neighbour and three smallest 3-body clusters were used). Numbers 1-3, 4-6, 7-9, 10-12 and 13-15 in Figure 3a denote pairs with 1st, 2nd, 3rd, 4th and 5th nearest neighbours respectively. Numbers 1-6, 7-12 and 13-18 in Figure 3b denote three smallest 3-body clusters. The strongest interactions have been observed between pairs with 1st and 2nd nearest neighbours, but strong interaction between pairs with 5th nearest neighbours has also been noted. Effective cluster interactions for Cr-W-Y system together with the description of considered clusters are given in Table 1.

Mapping DFT energies to CE was performed using the ATAT package [35]. Initial values of effective cluster interactions, derived by mapping to cluster expansion the DFT energies, provided a starting point for further refinement of the CE parameters, which was performed by generating new

Table 1. Effective cluster interactions for Cr-W-Y system. $|\omega|$, n, (s), $m^{(s)}_{|\omega|,n}$ and $J^{(s)}_{|\omega|,n}$ denote the cluster size, label, decoration of the cluster, multiplicity, and concentration-independent effective cluster interactions in meV, respectively.

$\|\omega\|$	n	(s)	Coordinates	$m^{(s)}_{\|\omega\|,n}$	$J^{(s)}_{\|\omega\|,n}$
1	1	(0)	(0,0,0)	1	538.452
		(1)		1	257.288
		(2)		1	211.843
2	1	(1,1)	(0, 0, 0; $\frac{1}{2}$, $\frac{1}{2}$, $\frac{1}{2}$)	4	-58.172
		(1,2)		8	-70.914
		(2,2)		4	-50.004
2	2	(1,1)	(0,0,0; 1,0,0)	3	-32.089
		(1,2)		6	-59.610
		(2,2)		3	-154.668
2	3	(1,1)	(0,0,0; 1,0,1)	6	3.656
		(1,2)		12	0.321
		(2,2)		6	-19.614
2	4	(1,1)	(0,0,0; 1$\frac{1}{2}$,$\frac{1}{2}$,$\frac{1}{2}$)	12	-5.678
		(1,2)		24	-7.450
		(2,2)		12	-27.653
2	5	(1,1)	(0,0,0; 1,1,1)	4	10.940
		(1,2)		8	32.636
		(2,2)		4	72.744
3	1	(1,1,1)	(1,0,0; $\frac{1}{2}$,$\frac{1}{2}$,$\frac{1}{2}$; 1,1,1)	12	-3.971
		(2,1,1)		24	-1.483
		(1,2,1)		12	-5.822
		(2,2,1)		24	0.522
		(2,1,2)		12	16.694
		(2,2,2)		12	27.950
3	2	(1,1,1)	($\frac{1}{2}$,-$\frac{1}{2}$,-$\frac{1}{2}$; 0,0,0; -$\frac{1}{2}$,-$\frac{1}{2}$,$\frac{1}{2}$)	12	3.509
		(2,1,1)		24	-3.726
		(1,2,1)		12	8.773
		(2,2,1)		24	-2.666
		(2,1,2)		12	-8.127
		(2,2,2)		12	-9.910
3	3	(1,1,1)		12	-4.250
		(2,1,1)		24	-2.652
		(1,2,1)		12	-1.870
		(2,2,1)		24	2.550
		(2,1,2)		12	-2.719
		(2,2,2)		12	4.426

structures. The resulting database for binary and ternary alloys consisted of 521 structures (3 pure elements, 431 binary and 87 ternary structures). The value of cross-validation error between DFT and CE formation enthalpies achieved during simulations was 15.8 meV/atom, proving that the final set of effective cluster interactions describes interatomic interactions in Cr-W-Y system accurately.

2.3. Chemical Short-Range Order Parameters

Monte Carlo simulations were carried out using a cell containing 2000 atoms in the form of 10x10x10 bcc unit cells. For each composition, simulations started from a disordered high-temperature state at 3000 K. The alloy was then quenched down to 100 K with a temperature step of ΔT = 100 K, with 2000 MC steps per atom at both thermalization and accumulation stages. In our study, we are using the Warren-Cowley Short-Range Order (SRO) parameters, which can be obtained from the pair probabilities as follows [36,37]:

$$\alpha_n^{ij} = 1 - \frac{y_n^{ij}}{c_i c_j} \tag{8}$$

where i and j are n-th nearest neighbour atoms, c_i and c_j the concentrations of atoms i and j, respectively. The y_n^{ij} values can be obtained by the matrix inversion from Eq. 5 following Ref. [38]. The SRO parameters can be calculated from the point and pair correlation functions. Point correlation functions are related to concentrations and do not change whereas pair correlation functions are averaged at each temperature over 2000 MC steps at the accumulation stage. Analytical formulas have been given in Ref. [39]. The expression to calculate the average SRO parameter for a bcc lattice for first and second nearest neighbours is [40]:

$$\alpha_{avg}^{ij} = \frac{8\alpha_1^{ij} + 6\alpha_2^{ij}}{14} \tag{9}$$

where α_1^{ij} and α_2^{ij} are the first and second nearest neighbours SRO parameters, respectively. SRO parameter values close to 0 indicate the presence of the fully disordered solid solution, positive values suggest the possibility of atomic segregation while negative values highlight the possibility of atomic ordering.

The configurational entropy contribution to the free energy of mixing has been computed using the pair probabilities from first nearest neighbours [41]:

$$S_{conf} = +7\sum_s y_{1,1}^{(s)}[\vec{\sigma}] log[y_{1,1}^{(s)}[\vec{\sigma}]] - 4\sum_s y_{2,1}^{(s)}[\vec{\sigma}] log[y_{2,1}^{(s)}[\vec{\sigma}]] \tag{10}$$

The entropy of mixing (S_{mix}), which indicates the effect of short-range ordering in reference to a random configuration, has been computed as:

$$S_{mix} = S_{rand} - S_{conf} \tag{11}$$

where S_{rand} is the entropy of a random configuration and is calculated using [28]:

$$S_{rand} = -k_B \sum_i c_i ln(c_i) \tag{12}$$

From Eqs. 10-12, we can then calculate the free energy of mixing from the analytical expression:

$$F_{mix} = H_{mix} - TS_{mix} \tag{13}$$

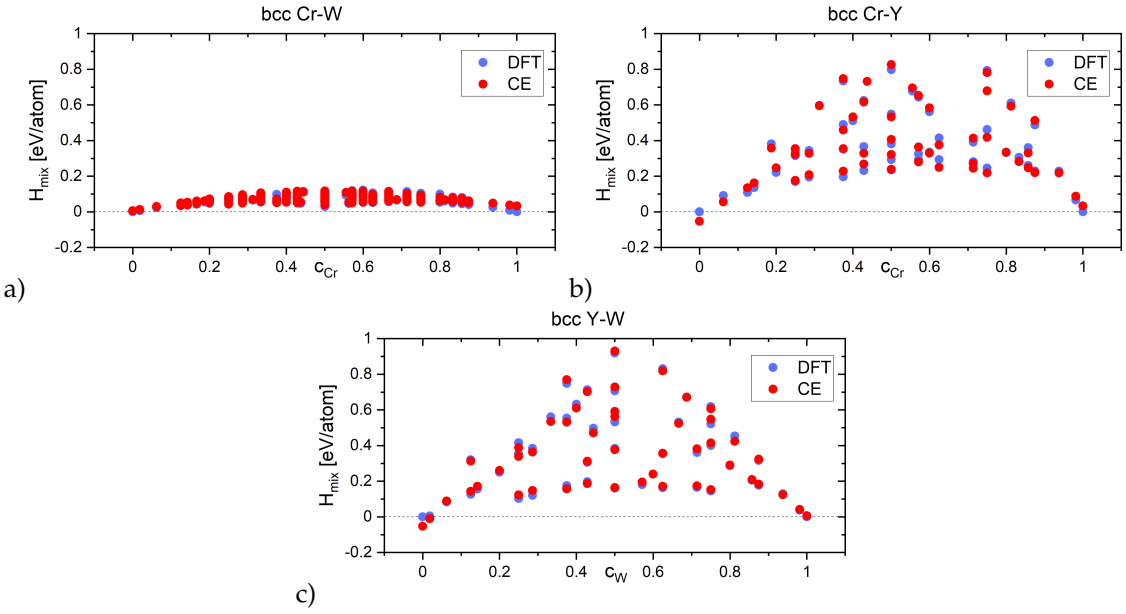

Figure 4. Enthalpies of mixing of bcc binary structures for a) Cr-W, b) Cr-Y and c) Y-W systems.

3. Phase stability of derivative Cr-W-Y alloys

3.1. Phase stability at 0 K

Enthalpies of mixing were calculated using DFT and CE methods for all 521 bcc structures in the obtained Cr-W-Y system database. The CE mapping was done for the whole 3-component system at once, not separately for each of the three subsystems. Enthalpies of mixing for all binary structures in the database were analysed in order to determine the nature of the interactions between atoms in all possible binary configurations. Enthalpy of mixing values close to 0 eV/atom indicate the possibility of solid solution creation, negative values indicate a tendency to forming intermetallic phases, while positive enthalpy of mixing values indicate the tendency towards atoms segregation. Enthalpy of mixing results for all binary alloys in Cr-W-Y systems are given in Figure 4. It has been observed that all structures in 3 binary systems in Cr-W-Y ternary system had positive enthalpies of mixing, with values for binary Cr-Y and Y-W systems reaching almost 1 eV/atom while being significantly higher than those for binary Cr-W (values up to 117 meV/atom). For all three binary systems, the most positive values of enthalpy of mixing are observed for structures with equal compositions of both elements.

3.2. Finite temperature phase stability and order-disorder transition temperatures of Cr-W-Y Smart Alloys

In Figure 5 the enthalpy of mixing as a function of temperature for $W_{70}Cr_{30}$, equiatomic WCrY and derivative $W_{70}Cr_{(30-x)}Y_x$, for $x = (0.5; 1; 1.5; 2)$ alloys is given. The lowest enthalpy of mixing values in the whole temperature range have been observed for $W_{70}Cr_{30}$ alloy, with values close to 0 meV/atom at 100 K, up to 63 meV/atom at 3000 K. It has been observed that even slight addition of yttrium (0.5 at.%) results in the significant increase of the enthalpy of mixing values in the whole temperature range. The $W_{70}Cr_{29.5}Y_0.5$ alloy has around 30 meV/atom higher enthalpy of mixing values than the $W_{70}Cr_{30}$ alloy. Further additions of Y up to 2 at.% did not result in significant enthalpy of mixing changes, with its values increasing by around 1 meV/atom per 0.5 at.% additional Y concentration.

We define the ODTT temperature as the temperature at which the alloy starts to become a fully disordered solid solution. In the present study it is calculated for each composition as the highest temperature at which the inflection point on the enthalpy of mixing as a function of temperature plot is present. It can also be calculated analysing the short-range order as a function of temperature. We

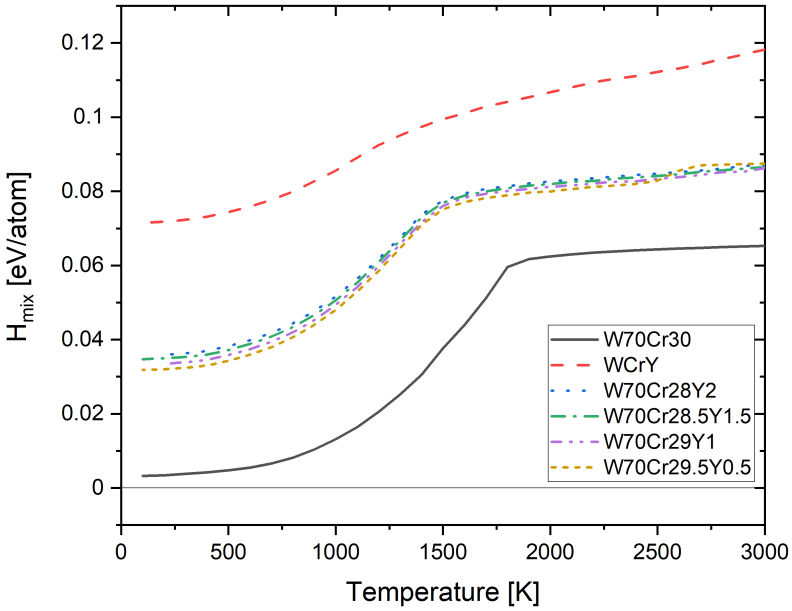

Figure 5. Enthalpy of mixing as a function of temperature for $W_{70}Cr_{30}$, equiatomic WCrY and derivative $W_{70}Cr_{(30-x)}Y_x$, for $x = (0.5; 1; 1.5; 2)$ alloys.

have found the inflection points of the enthalpy of mixing to be the same as those observed on SRO plots. In order to find the optimal composition with the lowest ODTT we analysed the influence of single elements as well as pairs of elements on the ODTT.

In Table 2 the order-disorder transition temperatures are given for equiatomic composition and several derivative alloy compositions considered in the Cr-Y-W system. alloys found in the Cr-Y-W system. The lowest ODTT have been observed for equiatomic alloy, 1100 K for WCrY. The $W_{70}Cr_{30}$ alloy, which serves as a baseline for understanding the influence of the additions of Y, has shown 1700 K ODTT. 0.5-2 at.% addition of Y has lowered the ODTT to 1300 K for $W_{70}Cr_{29.5}Y_{0.5}$, $W_{70}Cr_{29}Y_1$, $W_{70}Cr_{28.5}Y_{1.5}$ and $W_{70}Cr_{28}Y_2$ alloys, respectively.

Table 2. Order-disorder transition temperatures for alloys in Cr-W-Y system.

Alloy	*ODTT[K]*
$W_{70}Cr_{30}$	1700
WCrY	1100
$W_{70}Cr_{29.5}Y_{0.5}$	1300
$W_{70}Cr_{29}Y_1$	1300
$W_{70}Cr_{28.5}Y_{1.5}$	1300
$W_{70}Cr_{28}Y_2$	1300

3.3. Short-range ordering in derivative Cr-W-Y alloys

The Warren-Cowley SRO parameter was used to determine the derivation from random configuration toward ordering/segregation. The average SRO parameters were calculated using Eq. 9 for first and second nearest neighbours.

In Figure 6 the average short-range order parameters for $W_{70}Cr_{30}$, equiatomic WCrY, $W_{70}Cr_{29.5}Y_{0.5}$, $W_{70}Cr_{29}Y_1$, $W_{70}Cr_{28.5}Y_{1.5}$ and $W_{70}Cr_{28}Y_2$ alloys are given. It has been observed that for all five alloys containing Y, the SRO parameter values for the Cr-W pair are coming close 0 above 1500 K, while being positive below that temperature. The most positive SRO parameter values have

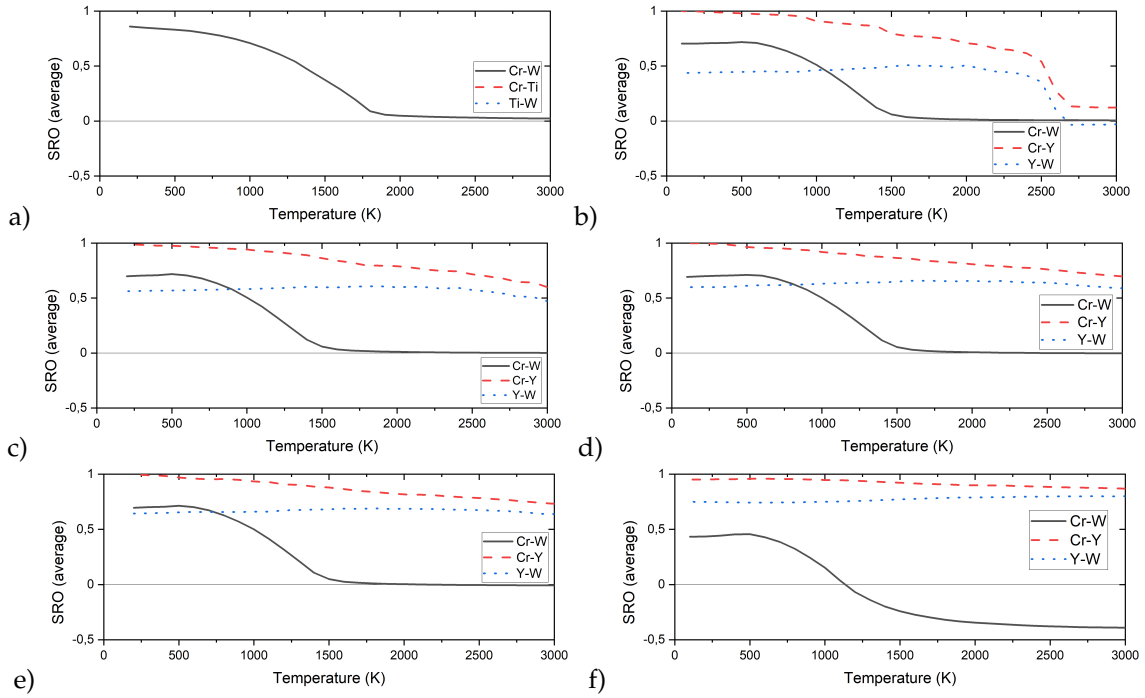

Figure 6. Average short-range order parameters for ternary a) $W_{70}Cr_{30}$, b) $W_{70}Cr_{29.5}Y_{0.5}$, c) $W_{70}Cr_{29}Y_1$, d) $W_{70}Cr_{28.5}Y_{1.5}$, e) $W_{70}Cr_{28}Y_2$ and f) WCrY alloys.

been observed for the Cr-Y pair. By comparing Figures 6b-e to Figure 6a, we have concluded that even small addition of Y (0.5 at.%) resulted in lowering the order-disorder transition temperature for the Cr-W pair from 1700 K for $W_{70}Cr_{30}$ to 1300 K for alloys containing 0.5-2 at.% of yttrium. We have not observed any significant differences in SRO parameters below 2500 K between four alloys presented in Figures 6b-e. In the equiatomic Cr-W-Y alloy (Figure 6f) both Cr-Y and Y-W pairs have shown very strong positive SRO parameter values even at high temperatures, indicating strong segregation between atoms in those pairs.

In Figure 7 image structures for the derivative $W_{70}Cr_{30}$, $W_{70}Cr_{29.5}Y_{0.5}$, $W_{70}Cr_{29}Y_1$, $W_{70}Cr_{28.5}Y_{1.5}$ and $W_{70}Cr_{28}Y_2$ alloys at three different temperatures (1000 K, 1400 K and 1800 K) are given. Very strong tendency towards clustering has been observed for Y atoms at 1000 K and 1400 K for all alloys containing Y (Figures 7a,d,g,j,m and Figures 7b,e,h,k,n). It has been noted, that at 1800 K for the $W_{70}Cr_{29.5}Y_{0.5}$ alloy, which contains the least amount of Y, there was no clustering of yttrium observed anymore. Based on the Figure 7 we concluded, that 1 at.% is the minimum concentration of Y required to observe the clustering at 1800 K (Figure 7i). In Figures 7a,b,c image structures for $W_{70}Cr_{30}$ alloy are given at 1000 K, 1400 K and 1800 K, respectively. It has been observed that there is a strong segregation between Cr and W atoms even at 1400 K, while in alloys containing Y there has been no segregation between Cr and W atoms observed. This is in agreement with with ODTT presented in Table 2, where it has been shown that the presence of Y in Cr-W alloys decreases the ODTT.

In Figure 8 the average SRO parameter values for Cr-W pair in $W_{70}Cr_{30}$, $W_{70}Cr_{29.5}Y_{0.5}$, $W_{70}Cr_{29}Y_1$, $W_{70}Cr_{28.5}Y_{1.5}$ and $W_{70}Cr_{28}Y_2$ alloys have been given. It has been observed that the addition of Y, even in very small concentration (0.5 at.%) had significant influence on the ordering of Cr-W pair. There has been observed a shift on the average SRO plot by around 400 K, resulting in lower ODTT for alloys with addition of Y (1300 K) compared to the $W_{70}Cr_{30}$ alloy (1700 K). These results are in agreement with ODTT derived from the enthalpies of mixing in Figure 5 and presented in Table 2. We have not observed any significant influence of continual increase of the Y concentration by 0.5 at.% up to 2 at.% on the Cr-W average SRO, compared to the alloy with 0.5 at.% yttrium.

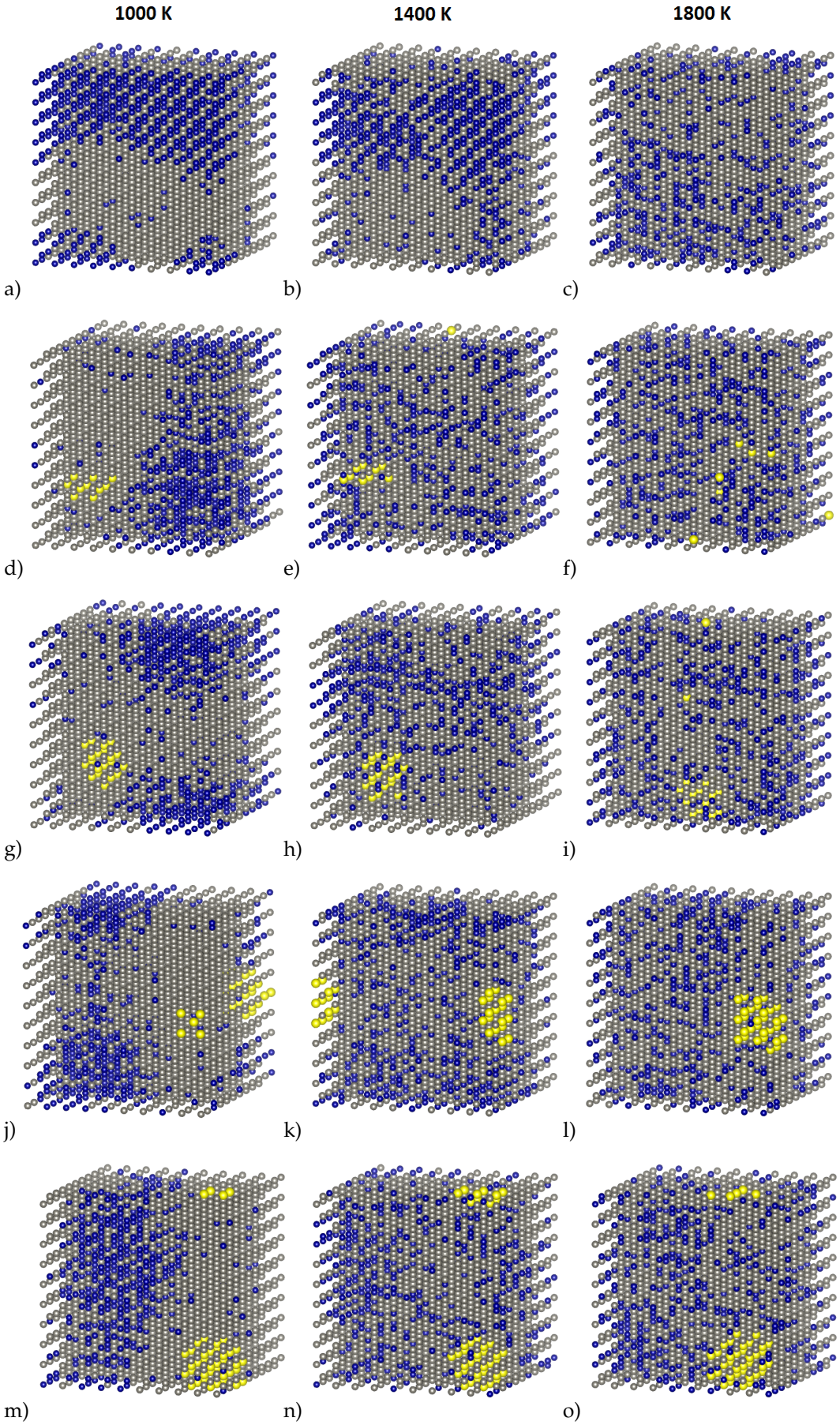

Figure 7. Structure images obtained from MC for a,b,c) $W_{70}Cr_{30}$, d,e,f) $W_{70}Cr_{29.5}Y_{0.5}$, g,h,i) $W_{70}Cr_{29}Y_1$, j,k,l) $W_{70}Cr_{28.5}Y_{1.5}$, m,n,o) $W_{70}Cr_{28}Y_2$ alloys at 1000 K (left column), 1400 K (middle column) and 1800 K (right column).

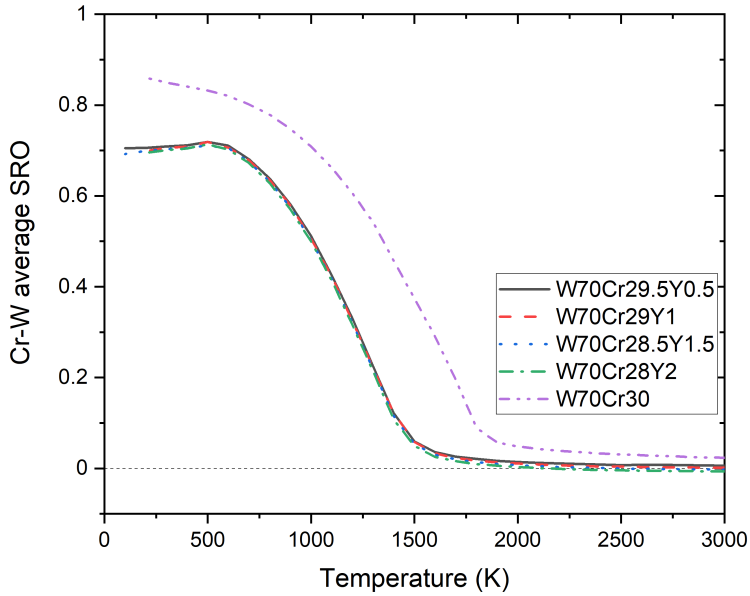

Figure 8. Cr-W average SRO comparison between $W_{70}Cr_{30}$ and derivative $W_{70}Cr_{(30-x)}Y_x$, for $x = (0.5; 1; 1.5; 2)$ alloys.

3.4. Free energy of mixing of derivative Cr-W-Y alloys.

In Figure 9 the free energy of mixing, entropy and enthalpy of mixing has been given for $W_{70}Cr_{29}Y_1$ alloy. Entropy contribution to the F_{mix} has been calculated using the 1st nearest neighbours approximation (1NN). Positive value of the free energy of mixing has been observed in the whole temperature range with values close to 0 at 1000 K to over 70 meV/atom at 3000 K.

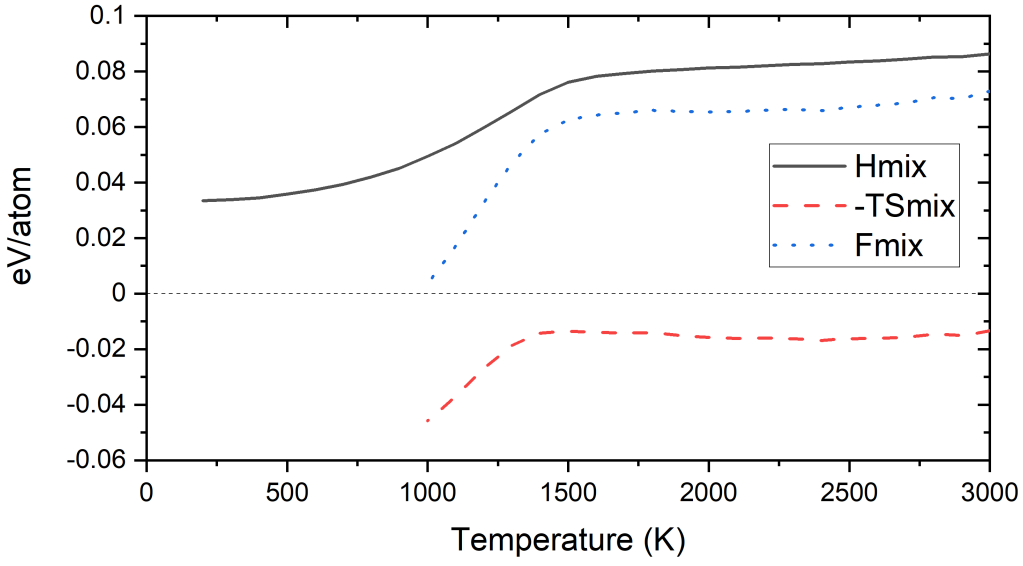

Figure 9. Free energy calculations from 1NN approximation for $W_{70}Cr_{29}Y_1$ alloy.

4. Phase stability of derivative Cr-Ti-W alloys

4.1. Phase stability at 0 K

Enthalpies of mixing were calculated by DFT and CE methods using our previously created model for quinary Cr-Ta-Ti-V-W system [26]. The CE mapping was done for the whole 5-component system

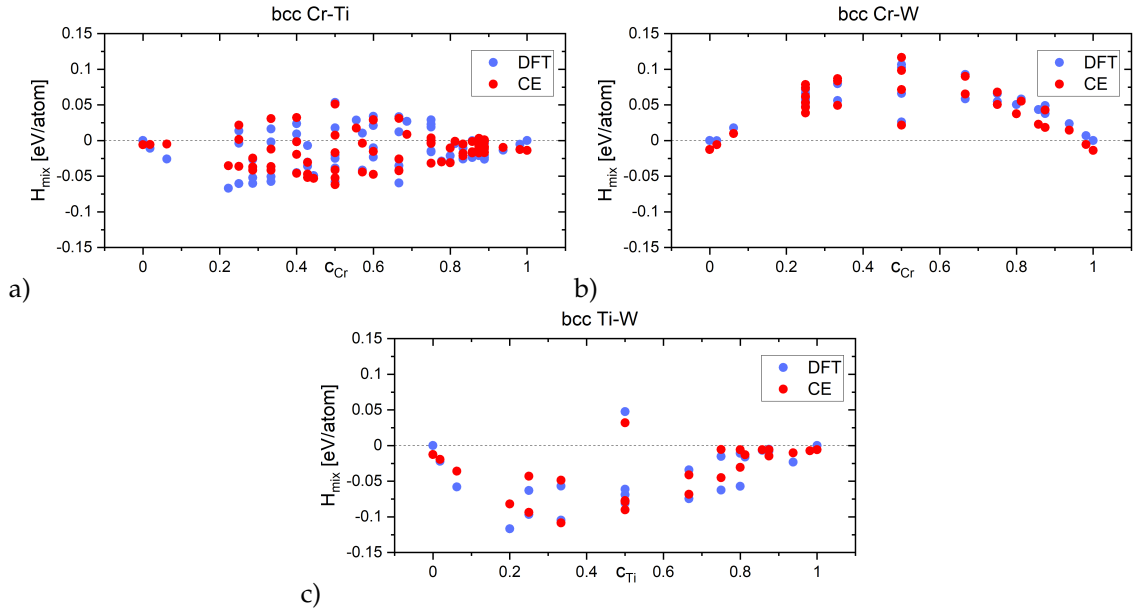

Figure 10. Enthalpies of mixing of bcc binary structures for a) Cr-Ti, b) Cr-W and c) Ti-W systems.

at once, not separately for each of the subsystems. Enthalpies of mixing for all binary structures in the database were analysed in order to determine the nature of the interactions between atoms in all possible binary configurations in ternary Cr-Ti-W system. The Cr-Ti binary system presents structures with both negative and positive values of enthalpies of mixing in the whole concentration range. The highest observed values were up to 50 meV/atom, while the lowest one (-67 meV/atom) was observed for the Cr_2Ti_7 structure. Almost all Cr-W structures had positive enthalpy of mixing, with highest up to 130 meV/atom. All but one structure found for the Ti-W system had negative enthalpy of mixing, with values as low as -117 meV/atom for the TiW_4 structure.

4.2. Finite temperature phase stability and order-disorder transition temperatures of Cr-Ti-W alloys

In Figure 11 the enthalpy of mixing as a function of temperature for $W_{70}Cr_{30}$, equiatomic WCrTi and derivative $W_{70}Cr_{(30-x)}Ti_x$, for $x = (0.5; 1; 1.5; 2)$ alloys is given. The lowest enthalpy of mixing in the whole temperature range has been observed for the equiatomic WCrTi alloy, with -69 meV/atom at 100 K up to -9 meV/atom at 3000 K. The highest enthalpy of mixing possess the $W_{70}Cr_{30}$ alloy, with 4 meV/atom at low temperatures, up to 66 meV/atom at 3000 K. By replacing 0.5 at.% of Cr with Ti, the enthalpy of mixing slightly decreased by around 2 meV/atom in the whole temperature range. Further addition of Ti in the place of Cr (up to 2 at.%) results in the same trend with the enthalpy of mixing decreasing by around 2 meV/atom for every 0.5 at.% of Ti added.

In Table 3 the order-disorder transition temperatures are given for several equiatomic and derivative alloys found in the Cr-Ti-W system. The lowest ODTT have been observed for equiatomic alloy, namely 900 K for WCrTi. The $W_{70}Cr_{30}$ alloy, which serves as a baseline for understanding the influence of the additions of Ti and Y, has shown 1700 K ODTT. The addition of Ti has not shown any influence on the ODTT.

Table 3. Order-disorder transition temperatures for alloys in Cr-Ti-W system.

Alloy	*ODTT[K]*
$W_{70}Cr_{30}$	1700
WCrTi	900
$W_{70}Cr_{29.5}Ti_{0.5}$	1700
$W_{70}Cr_{29}Ti_1$	1700
$W_{70}Cr_{28.5}Ti_{1.5}$	1700
$W_{70}Cr_{28}Ti_2$	1700

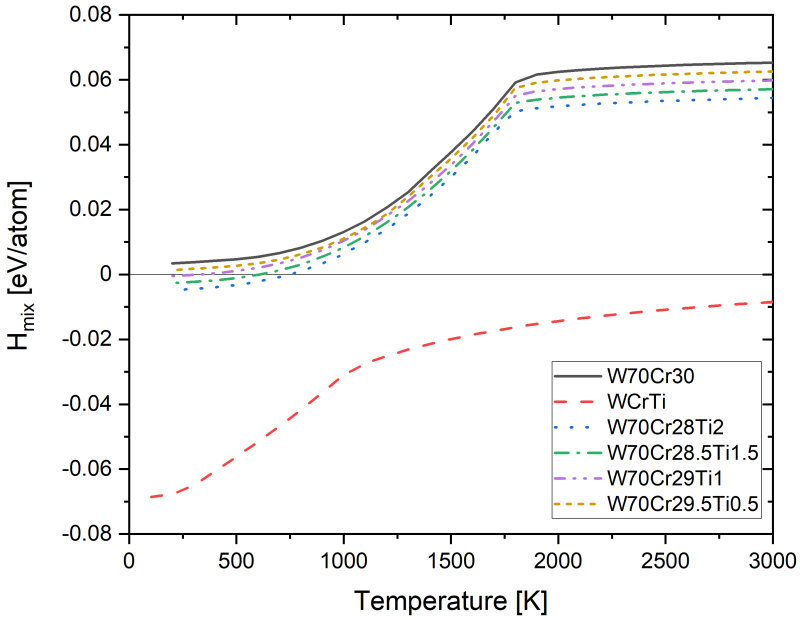

Figure 11. Enthalpy of mixing as a function of temperature for $W_{70}Cr_{30}$, equiatomic WCrTi and derivative $W_{70}Cr_{(30-x)}Ti_x$, for $x = (0.5; 1; 1.5; 2)$ alloys.

4.3. Short-range ordering in derivative Cr-Ti-W alloys

In Figure 12 the average short-range order parameters for ternary $W_{70}Cr_{29.5}Ti_{0.5}$, $W_{70}Cr_{29}Ti_1$, $W_{70}Cr_{28.5}Ti_{1.5}$, $W_{70}Cr_{28}Ti_2$ and equiatomic WCrTi alloys are given. Negative values of the SRO parameter have been observed for Ti-W pair below 1800 K indicating attraction between those atoms, while both Cr-Ti and Cr-W have shown strongly positive SRO parameter values below 1800 K. We have not observed any differences in Cr-W pair behaviour in $W_{70}Cr_{30}$ alloy (Figure 6a) compared to alloys containing up to 2 at.% of Ti (Figures 12a-d).

In Figure 13 structure images for $W_{70}Cr_{29}Ti_1$ alloy at 1000 K, 1400 K and 1800 K have been given. It has been observed, that contrary to the behaviour of Y, Ti is not forming Ti-rich clusters even at low temperatures. Ti atoms are mostly spread within the W-rich regions, which is consistent with results presented in Figure 12b, where it has been shown that the Ti-W pair has negative SRO parameter and thus tendency to attract each other.

In Figure 14 the average SRO parameter values for Cr-W pair in $W_{70}Cr_{30}$, $W_{70}Cr_{29.5}Ti_{0.5}$, $W_{70}Cr_{29}Ti_1$, $W_{70}Cr_{28.5}Ti_{1.5}$ and $W_{70}Cr_{28}Ti_2$ alloys have been given. It has been observed that the addition of Ti, did not have any significant influence on the ordering of Cr-W pair compared to the $W_{70}Cr_{30}$. The observed ODTT has been the same for all analysed alloys (1700 K) and is agreement with the ODTT derived from enthalpies of mixing (Figure 11) and presented in Table 3.

4.4. Free energy of mixing of derivative Cr-Ti-W alloys.

In Figure 15 the free energy of mixing, entropy and enthalpy of mixing has been given for $W_{70}Cr_{29}Ti_1$ alloy. Entropy contribution to the F_{mix} has been calculated using the 1st nearest neighbours approximation (1NN). A negative value of the free energy of mixing has been observed below 1300 K, as low as -40 meV/atom at 1000 K, and positive above 1300 K up to 52 meV/atom at 3000 K.

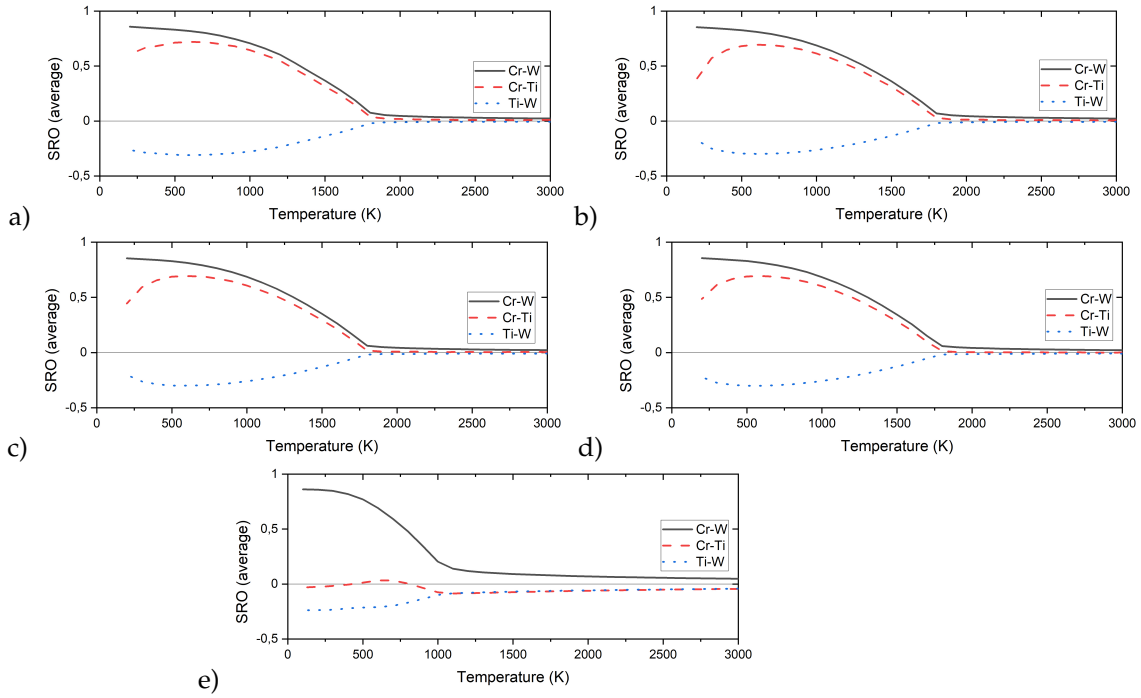

Figure 12. Average short-range order parameters for ternary a) $W_{70}Cr_{29.5}Ti_{0.5}$, b) $W_{70}Cr_{29}Ti_1$, c) $W_{70}Cr_{28.5}Ti_{1.5}$, d) $W_{70}Cr_{28}Ti_2$ and e) WCrTi alloys.

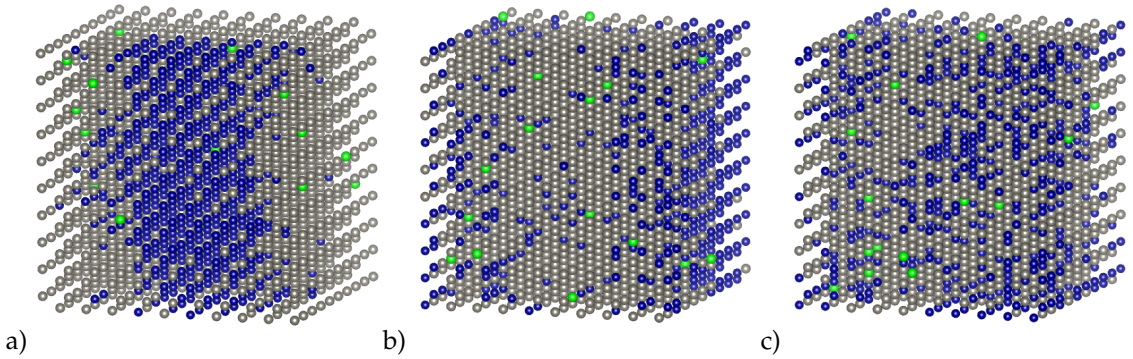

Figure 13. Structure images obtained from MC for $W_{70}Cr_{29}Ti_1$ alloy at a) 1000 K, b) 1400 K and c) 1800 K. W (grey), Cr (blue), Ti (green).

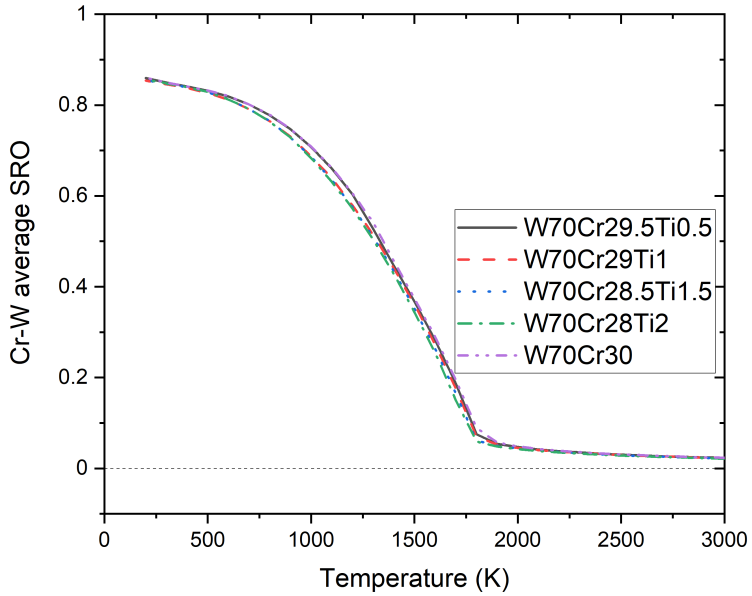

Figure 14. Cr-W average SRO comparison between $W_{70}Cr_{30}$ and derivative $W_{70}Cr_{(30-x)}Ti_x$, for $x = (0.5; 1; 1.5; 2)$ alloys.

5. Conclusions

A DFT-based Cluster Expansion model has been developed for the ternary bcc Cr-W-Y system. All binary structures investigated in this system from DFT calculations showed positive enthalpies of mixing, with Cr-Y and W-Y pairs being much more positive than Cr-W pairs. Previously developed model for quinary Cr-Ta-Ti-V-W system has been used to analyse ternary Cr-Ti-W alloys. Most of the Cr-Ti and Ti-W binary structures had negative values of the enthalpy of mixing.

CE Hamiltion for MC simulations has been developed to analyse the phase stability and the short-range ordering in the derivative $W_{70}Cr_{(30-x)}Y_x$ (for $x = (0.5; 1; 1.5; 2)$) alloys. Addition of Y to $W_{70}Cr_{30}$ alloy, even at very low concentrations, resulted in the decrease of the ordering between Cr and W by 400 K from 1700 K to 1300 K. Strong tendency towards clustering at elevated temperatures, as high as the 1800 K, has been observed for Y atoms in alloys containing at least 1 at.% yttrium.

Monte-Carlo simulations for derivative ternary $W_{70}Cr_{(30-x)}Ti_x$ (for $x = (0.5; 1; 1.5; 2)$) alloys based on the previously created Cr-Ta-Ti-V-W system have been carried out to compare the influence of the Ti on the ordering in $W_{70}Cr_{30}$ alloy. The addition of Ti has not shown any influence on the ODTT of analysed alloys, as the ODTT for alloys containing between 0.5 at.% and 2 at.% of Ti had ODTT of 1700 K, same as the $W_{70}Cr_{30}$ alloy.

The difference in the ODTT and clustering of the $W_{70}Cr_{29}Y_1$ alloy compared to the $W_{70}Cr_{(30-x)}Ti_x$ alloy can be explained by the nature of interactions between atoms in those alloys. As shown in Figure 12, the SRO parameter for Ti-W pair is negative which results in Ti atoms to be present inside W-rich regions and it can be observed in Figure 13. The attraction between Ti and W inhibits formation of Ti-rich clusters. The SRO parameter is positive for all pairs in Cr-W-Y system, which results in separation between Cr-rich, W-rich and Y-rich regions and favors Y-rich clusters formation.

Our MC simulations showed that for the $W_{70}Cr_{29}Y_1$ alloy the enthalpy of mixing value is positive in the whole analysed temperature range. Free energy of mixing has also been derived from the first nearest neighbours approximation for the $W_{70}Cr_{29}Y_1$ and $W_{70}Cr_{29}Ti_1$ alloys, at temperatures above 1000 K. It has been found out, that for the $W_{70}Cr_{29}Y_1$ alloy the F_{mix} value is positive in the whole analysed temperature range, while for the $W_{70}Cr_{29}Ti_1$ the F_{mix} is negative below 1300 K.

The results of the present investigations provide an insight enabling for optimizing chemical composition of materials for future plasma facing components. The differences between yttrium and

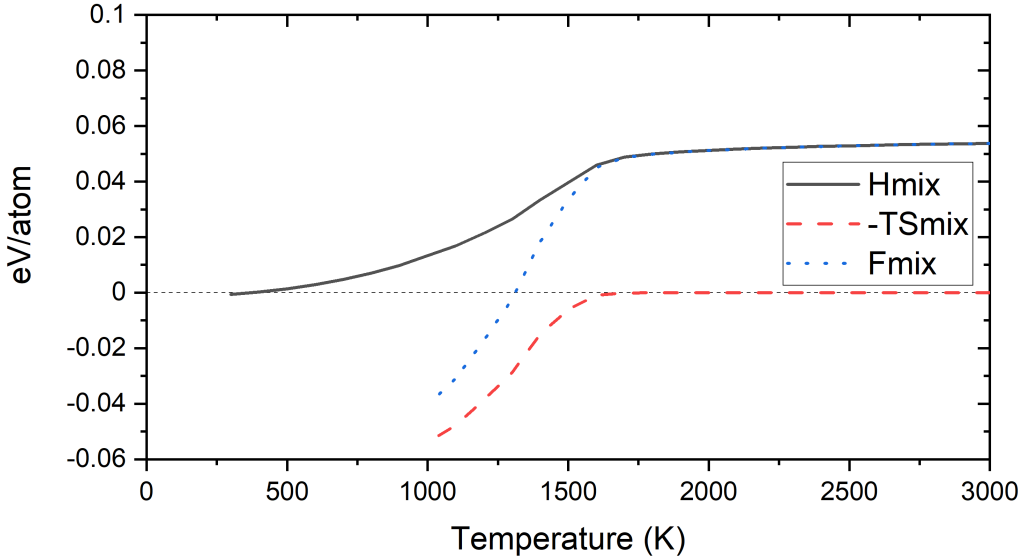

Figure 15. Free energy calculations from 1NN approximation for $W_{70}Cr_{29}Ti_1$ alloy.

titanium influence on the Cr-W phase stability may be found helpful for selecting alloying elements beyond Ti/Y for PFM. Present study suggests, that highly positive values of the enthalpy of mixing between the alloying element and Cr/W, may result in the decrease of the ODTT of studied alloys.

Author Contributions: Conceptualization, D.S., J.S.W., M.R.G., A.L., F.K., K.J.K. and D.N.-M.; Methodology, D.S., J.S.W. and D.N.-M.; Validation, J.S.W., A.L. and D.N.-M.; Formal Analysis, D.S., J.S.W. and D.N.-M.; Investigation, D.S., J.S.W., M.R.G., A.L., F.K., K.J.K. and D.N.-M.; Resources, J.S.W. and D.N.-M.; Data Curation, D.S. and J.S.W.; Writing – Original Draft Preparation, D.S., J.S.W., M.R.G. and D.N.-M.; Writing – Review & Editing, D.S., J.S.W., M.R.G., A.L., F.K., K.J.K. and D.N.-M.; Visualization, D.S. and M.R.G.; Supervision, J.S.W., A.L. and D.N.-M.; Project Administration, J.S.W., A.L. and D.N.-M.; Funding Acquisition, J.S.W., A.L. and D.N.-M.

Funding: The work at Warsaw University of Technology has been carried out as a part of an international project co-financed from the funds of the program of the Polish Minister of Science and Higher Education entitled "PMW" in 2019; Agreement No. 5018 / H2020-Euratom / 2019/2. The simulations were also carried out with the support of the Interdisciplinary Centre for Mathematical and Computational Modelling (ICM), University of Warsaw, under grant No. GB79-6.

This work has been carried out within the framework of the EUROfusion Consortium and has received funding from the Euratom research and training programme 2014-2018 and 2019-2020 under grant agreement No 633053. MRG and DNM acknowledge funding from the RCUK [grant number EP/T012250/1].

Acknowledgments: JSW and DNM would like to acknowledge the support from high-performing computing facility MARCONI (Bologna, Italy) provided by EUROfusion.

The views and opinions expressed herein do not necessarily reflect those of the European Commission

Conflicts of Interest: The authors declare no conflict of interest.

Abbreviations

The following abbreviations are used in this manuscript:

1NN - First Nearest Neighbours
BCC - Body-Centered Cubic
CE - Cluster Expansion
DFT - Density Functional Theory
LLW - Low Level Waste
LOCA - Loss-Of-Coolant Accident
MC - Monte Carlo
ODTT - Order-Disorder Transition Temperature
PFM - Plasma-Facing-Materials
PAW - Projector Augmented Wave
SRO - Short-Range Order

References

1. Klein, F.; Gilbert, M.R.; Litnovsky, A.; Gonzalez-Julian, J.; Weckauf, S.; Wegener, T.; Schmitz, J.; Linsmeier, Ch.; Bram, M.; Coenen, J.W., Tungsten–chromium–yttrium alloys as first wall armor material: Yttrium concentration, oxygen content and transmutation elements, **2020**, *Fusion Eng. Des.*, *158*, 111667; DOI:10.1016/j.fusengdes.2020.111667
2. Litnovsky, A.; Schmitz, J.; Klein, F.; De Lannoye, K.; Kreter, A.; Rasinski, M.; Coenen, J.W.; Linsmeier, Ch.; Gonzalez-Julian, J.; Bram, M.; Povstugar, I.; Morgan, T.; Nguyen-Manh, D.; Gilbert, M.R.; Sobieraj, D.; Wróbel, J.S., Smart Tungsten-based Alloys for a First Wall of DEMO, **2020**, *Fusion Eng. Des.* , *159*, 111742, DOI:10.1016/j.fusengdes.2020.111742
3. Lloyd, M.J.; Abernethy, R.G.; Gilbert, M.R.; Griffiths, I.; Bagot, P.A.J.; Nguyen-Manh, D.; Moody, M.P.; Armstrong, D.E.J., Decoration of voids with rhenium and osmium transmutation products in neutron irradiated single crystal tungsten, **2019** *Scr. Mater.*, *173*, 96–100; DOI:10.1016/j.scriptamat.2019.07.036
4. El-Atwani, O.; Li, N.; Li, M.; Devaraj, A.; Baldwin, J.K.S.; Schneider, M.M.; Sobieraj, D.; Wróbel, J.S.; Nguyen-Manh, D.; Maloy, S.A.; Martinez, E., Outstanding radiation resistance of tungsten-based high-entropy alloys, **2019** *Sci. Adv.*, *5*, aav2020; DOI:10.1126/sciadv.aav2002
5. Gilbert, M.R.; Eade, T.; Bachmann, C.; Fischer, U.; Taylor, N.P., Activation, decay heat, and waste classification studies of the European DEMO concept, **2017**, *Nucl. Fusion*, *57(4)*, 046015; DOI:10.1088/1741-4326/aa5bd7
6. Schmitz, J.; Litnovsky, A.; Klein, F.; De Lannoye, K.; Kreter, A.; Rasinski, M.; Breuer, U.; Gonzalez-Julian, J.; Bram, M.; Coenen, J.W.; Linsmeier, Ch., On the plasma suitability of WCrY smart alloys—the effect of mixed D+Ar/He plasmas, **2020**, *Phys. Scr.*, *T171*, 014002; DOI:10.1088/1402-4896/ab367c
7. Schmitz, J.; Litnovsky, A.; Klein, F.; Tan, X.Y.; Breuer, U.; Rasinski, M.; Ertmer, S.; Kreter, A.; Gonzalez-Julian, J.; Bram, M.; Coenen, J.W.; Linsmeier, Ch., Argon-seeded plasma exposure and oxidation performance of tungsten-chromium-yttrium smart alloys, **2019**, *Tungsten*, *1*, 1–3; DOI:10.1007/s42864-019-00016-7
8. Klein, F.; Litnovsky, A.; Wegener, T.; Tan, X.Y.; Gonzalez-Julian, J.; Rasinski, M.; Schmitz, J.; Linsmeier, Ch.; Bram, M.; Coenen, J.W., Sublimation of advanced tungsten alloys under DEMO relevant accidental conditions, **2019**, *Fusion Eng. Des.*, *146A*, 1198–1202; DOI:10.1016/j.fusengdes.2019.02.039
9. Tan, X.Y.; Klein, F.; Litnovsky, A.; Wegener, T.; Schmitz, J.; Linsmeier, Ch.; Coenen, J.W.; Breuer, U.; Rasinski, M.; Li, P.; Luo, L.M.; Wu, Y.C., Evaluation of the high temperature oxidation of W-Cr-Zr self-passivating alloys, **2019**, *Corros. Sci.*, *147*, 201–211; DOI:10.1016/j.corsci.2018.11.022
10. Klein, F.; Wegener, T.; Litnovsky, A.; Rasinski, M.; Tan, X.Y.; Schmitz, J.; Linsmeier, Ch.; Coenen, J.W.; Du, H.; Mayer, J.; Breuer, U., On Oxidation Resistance Mechanisms at 1273 K of Tungsten-Based Alloys Containing Chromium and Yttria, **2018**, *Metals*, *8*, 488; DOI:10.3390/met8070488
11. Klein, F.; Wegener, T.; Litnovsky, A.; Rasinski, M.; Tan, X.Y.; Gonzalez-Julian, J.; Schmitz, J.; Bram, M,.;Coenen, J.W.; Linsmeier, Ch., Oxidation resistance of bulk plasma-facing tungsten alloys, **2018**, *Nucl. Mater. Energy*, *15*, 226–231; DOI:10.1016/j.nme.2018.05.003
12. Litnovsky, A.; Wegener, T.; Klein, F.; Linsmeier, Ch.; Rasinski, M.; Kreter, A.; Tan, X.Y.; Schmitz, J.; Mao, Y.; Coenen, J.W.; Bram, M.; Gonzalez-Julian, J., Oxidation resistance of bulk plasma-facing tungsten alloys, **2017**, *Plasma Phys. Control. Fusion*, *59*, 064003; DOI:10.1016/j.nme.2018.05.003
13. Litnovsky, A.; Wegener, T.; Klein, F.; Linsmeier, Ch.; Rasinski, M.; Kreter, A.; Unterberg, B.; Coenen, J.W.; Du, H.; Mayer, J.; Garcia-Rosales, C.; Calvo, A.; Ordas, N., Smart tungsten alloys as a material for the first wall of a future fusion power plant, **2017**, *Nucl. Fusion*, *57*, 066020; DOI:10.1088/1741-4326/aa6816
14. Fischer, U.; Bachmann, C.; Catalan, J.P.; Eade, T.; Flammini, D.; Gilbert, M.R.; Jaboulay, J.-Ch.; Konobeev, A.; Leichtle, D.; Lu, L,; Malouch, F.; Moro, F.; Pereslavtsev, P.; Qiu, Y.; Sanz, L.; Sauvan, P.; Stankunas, G.; Travleev, A.; Turner, A.; Ogando, F.; Palermo, I.; Villari, R.;, Methodological approach for DEMO neutronics in the European PPPT programme: Tools, data and analyses, **2017**, *Fusion Eng. Des.*, *123*, 26–31; DOI:10.1016/j.fusengdes.2017.01.053
15. Federici, G.; Biel, W.; Gilbert, M.R.; Kemp, R.; Taylor, N.; Wenninger, R., European DEMO design strategy and consequences for materials, **2017**, *Nucl. Fusion*, *57*, 092002; DOI:10.1088/1741-4326/57/9/092002
16. Federici, G.; Bachmann, C.; Barucca, L.; Biel, W.; Boccaccini, L.; Brown, R.; Bustreo, C.; Ciattaglia, S.; Cismondi, F.; Coleman, M.; Corato, V.; Day, C.; Diegele, E.; Fischer, U.; Franke, T.; Gliss, C.; Ibarra, A.; Kembleton, R.; Loving, A.; Maviglia, F.; Meszaros, B.; Pintsuk, G.; Taylor, N.; Tran, M.Q.; Vorpahl, C.;

Wenninger, R.; You, J.H., DEMO design activity in Europe : progress and updates, **2018**, *Fusion Eng. Des.*, *136*, 729–741; DOI:10.1016/j.fusengdes.2018.04.001

17. Sublet, J.-Ch.; Eastwood, J.W.; Morgan, J.G.; Gilbert, M.R.; Fleming, M.; Arter, W., FISPACT-II: An Advanced Simulation System for Activation, Transmutation and Material Modelling, **2017**, *Nucl. Data Sheets*, *139* 77–137; DOI:10.1016/j.nds.2017.01.002
18. Koning, A.J.; Rochman, D.; Sublet, J. TENDL-2019; Release Date: December 31, **2019**. Available from https://tendl.web.psi.ch/tendl_2019/tendl2019.html
19. Gilbert, M. R.; Eade, T.; Rey, T.; Vale, R.; Bachmann, C.; Fischer, U.; Taylor, N., Waste implications from minor impurities in European DEMO materials, **2019**, *Nucl. Fus.*, *59* 076015; DOI:10.1088/1741-4326/ab154e
20. Gilbert, M.R.; Sublet, J. -Ch, Handbook of activation, transmutation, and radiation damage properties of the elements simulated using FISPACT-II & TENDL-2015; Magnetic Fusion Plants, CCFE-R(16)36, UKAEA, **2016** available from http://fispact.ukaea.uk
21. Blöchl, P.E., Projector augmented-wave method, **1994**, *Phys. Rev. B*, *50*, 17953–17978; DOI:10.1103/PhysRevB.50.17953
22. Kresse, G.; Furthmiiller, J., Efficient iterative schemes for ab initio total-energy calculations using a plane-wave basis set, **1996**, *Phys. Rev. B*, *54*, 11169; DOI:10.1103/PhysRevB.54.11169
23. Kresse, G.; Furthmiiller, J., Efficiency of ab-initio total energy calculations for metals and semiconductors using a plane-wave basis set, **1996**, *Comput. Mater. Sci.*, *6*, 15–50; DOI:10.1016/0927-0256(96)00008-0
24. Hafner, J., Ab-initio simulations of materials using VASP: Density-functional theory and beyond, **2008**, *J. Comput. Chem.*, *29*, 2044–2078; DOI:10.1002/jcc.21057;
25. Perdew, J.P.; Burke, K.; Ernzerhof, M., Generalized Gradient Approximation Made Simple, **1997**, *Phys. Rev. Lett.*, *77*, 3865; DOI:10.1103/PhysRevLett.77.3865
26. Sobieraj, D.; Wróbel, J.S.; Rygier, T.; Kurzydłowski, K.J.; El-Atwani, O.; Devaraj, A.; Martinez, E.; Nguyen-Manh, D., Chemical short-range order in derivative Cr–Ta–Ti–V–W high entropy alloys from the first-principles thermodynamic study, **2020**, *Phys. Chem. Chem. Phys.*, *22*, 23929; DOI:10.1039/D0CP03764H
27. Monkhorst, H.J.; Pack, J.D., Special points for Brillouin-zone integrations, **1976**, *Phys. Rev. B*, *13*, 5188; DOI:10.1103/PhysRevB.13.5188
28. Wróbel, J.S.; Nguyen-Manh, D.; Lavrentiev, M.Y.; Muzyk, M.; Dudarev, S.L., Phase stability of ternary fcc and bcc Fe-Cr-Ni alloys, **2015**, *Phys. Rev. B*, *91*, 024108; DOI:10.1103/PhysRevB.91.024108
29. de Fontaine, D., The number of independent pair-correlation functions in multicomponent systems, **1971**, *J. Appl. Crystallogr.*, *4*, 15–19; DOI:10.1107/S0021889871006174
30. Sanchez, J.M.; Ducastelle, F.; Gratias, D., Generalized cluster description of multicomponent systems, **1984**, *Physica A*, *128*, 334–350; DOI:10.1016/0378-4371(84)90096-7
31. Sanchez, J.M., Foundations and Practical Implementations of the Cluster Expansion, **2017**, *J. Phase Equilibria Diffus.*, *38*, 238–251; DOI:10.1007/s11669-017-0521-3
32. Wu, Q.; He, B.; Song, T.; Gao, J.; Shi, S., Cluster expansion method and its application in computational materials science, **2016**, *Comput. Mater. Sci.*, *125*, 243–254; DOI:10.1016/j.commatsci.2016.08.034
33. Chinnappan, R.; Panigrahi, B.K.; van de Walle, A., First-principles study of phase equilibrium in Ti–V, Ti–Nb, and Ti–Ta alloys, **2016**, *Calphad*, *54*, 125–133; DOI:10.1016/j.calphad.2016.07.001
34. Connolly, J.W.D.; Williams, A.R., Density-functional theory applied to phase transformations in transition-metal alloys, **1983**, *Phys. Rev. B*, *27*, 5169; DOI:10.1103/PhysRevB.27.5169
35. van de Walle, A.; Asta, M.; Ceder, G., The alloy theoretic automated toolkit: A user guide, **2002**, *Calphad*, *26*, 539–553; DOI:10.1016/S0364-5916(02)80006-2
36. Warren, B.E., X-ray diffraction, **1990**, *New York: Dover*
37. Cowley, J.M., An Approximate Theory of Order in Alloys, **1950**, *Phys. Rev.*, *77*, 669; DOI:10.1103/PhysRev.77.669
38. Fernández-Caballero, A.; Fedorov, M.; Wróbel, J.S.; Mummery, P.M.; Nguyen-Manh, D., Configurational Entropy in Multicomponent Alloys: Matrix Formulation from Ab Initio Based Hamiltonian and Application to the FCC Cr-Fe-Mn-Ni System, **2019**, *Entropy*, *21*, 68; DOI:10.3390/e21010068
39. Fernández-Caballero, A.; Wróbel, J.S.; Mummery, P.M.; Nguyen-Manh, D., Short-Range Order in High Entropy Alloys: Theoretical Formulation and Application to Mo-Nb-Ta-V-W System, **2017**, *J. Phase Equilibria Diffus*, *38*, 391–403; DOI:10.1007/s11669-017-0582-3

40. Mirebeau, I.; Hennion, M.; Parette, G., First Measurement of Short-Range-Order Inversion as a Function of Concentration in a Transition Alloy, **1984**, *Phys. Rev. Lett.*, *53*, 687–690; DOI:10.1103/PhysRevLett.53.687
41. Fedorov, M.; Wróbel, J.S.; Fernadez-Caballero, A.; Kurzydłowski, K.J.; Nguyen-Manh, D., Phase stability and magnetic properties in fcc Fe-Cr-Mn-Ni alloys from first-principles modeling, **2020**, *Phys. Rev. B*, *101*, 174416; DOI:10.1103/PhysRevB.101.174416